Focal adhesions are hotspots for keratin filament precursor formation

Reinhard Windoffer, Anne Kölsch, Stefan Wöll, and Rudolf E. Leube

Department of Anatomy and Cell Biology, Johannes Gutenberg University, 55128 Mainz, Germany

Recent studies showed that keratin filament (KF) formation originates primarily from sites close to the actin-rich cell cortex. To further characterize these sites, we performed multicolor fluorescence imaging of living cells and found drastically increased KF assembly in regions of elevated actin turnover, i.e., in lamellipodia. Abundant KF precursors (KFPs) appeared within these areas at the distal tips of actin stress fibers, moving alongside the stress fibers until their integration into the peripheral KF network. The earliest KFPs were detected next to actin-anchoring focal adhesions (FAs) and were only seen after the establishment of FAs in emerging lamellipodia. Tight spatiotemporal coupling of FAs and KFP formation were not restricted to epithelial cells, but also occurred in non-epithelial cells and cells producing mutant keratins. Finally, interference with FA formation by talin short hairpin RNA led to KFP depletion. Collectively, our results support a major regulatory function of FAs for KF assembly, thereby providing the basis for coordinated shaping of the entire cytoskeleton during cell relocation and rearrangement.

Introduction

Keratins are polypeptide components of the epithelial intermediate filament (IF) cytoskeleton that contribute to tissue homeostasis as important protective factors to combat various types of stress (Coulombe and Omary, 2002; Herrmann et al., 2003). The intrinsically rigid IF system must adapt to changing structural requirements in cells undergoing reshaping during development, cell division, migration, or metastasis. In contrast to microtubules and actin filaments, however, comparatively little is known about the molecular mechanisms governing the dynamic properties of IFs. Their assembly from nonpolar tetrameric building blocks and their propensity to spontaneously assemble without additional cofactors in vitro (Herrmann and Aebi, 2004) suggest unique organizational principles. Molecular details of the in vivo assembly and turnover are understood even less, although it is generally agreed that phosphorylation is important (Coulombe and Omary, 2002). Imaging of living cells producing fluorescent keratins has provided evidence for the importance of phosphorylation (Strnad et al., 2002) and has led to novel concepts about the spatial and temporal specifications of keratin filament (KF) dynamics. Thus, it was shown that KF network formation and turnover are dictated by the cell periphery with nascent KF precursors (KFPs) appearing in close proximity to the actin-rich cell cortex, followed by KFP elongation and their transport toward the cell interior before network assembly (Windoffer and Leube, 2001; Windoffer et al., 2004). This process is independent of cellular differentiation and may also be relevant to other IFs (Windoffer et al., 2004; Wöll et al., 2005). The dynamic properties of KFs and other IF systems are further determined by their association with the microtubule and actin filament systems (for reviews see Leung et al., 2002; Helfand et al., 2003). This linkage becomes particularly apparent in situations when either of the other systems is destroyed, thereby uncovering two types of KFP motility: a comparatively slow, continuous, and inward-directed actin-dependent movement and a fast, intermittent, and bidirectional motility that is dependent on an intact microtubule system (Wöll et al., 2005).

Considering the predominant formation of KFPs in proximity to the actin-rich cortex and the transport of KFPs in an actin-dependent fashion, we decided to examine the possibility that KFP formation is linked to the peripheral actin system and its associated adhesion structures.

Results and discussion

KF network formation is induced in lamellipodia

To examine the interrelationship between the actin system and the formation and transport of KFPs, we focused on lamellipodia, because they are rich in cortical actin, actin stress fibers, and

R. Windoffer and A. Kölsch contributed equally to this paper.

Correspondence to Rudolf E. Leube: leube@uni-mainz.de

Abbreviations used in this paper: ECFP, enhanced CFP; EYFP, enhanced YFP; IF, intermediate filament; FA, focal adhesion; HK, human keratin; KF, keratin filament; KFP, KF precursor; RFP, red fluorescent protein; shRNA, short hairpin RNA.

The online version of this article contains supplemental materials.

The Journal of Cell Biology, Vol. 173, No. 3, May 8, 2006 341–348
http://www.jcb.org/cgi/doi/10.1083/jcb.200511124

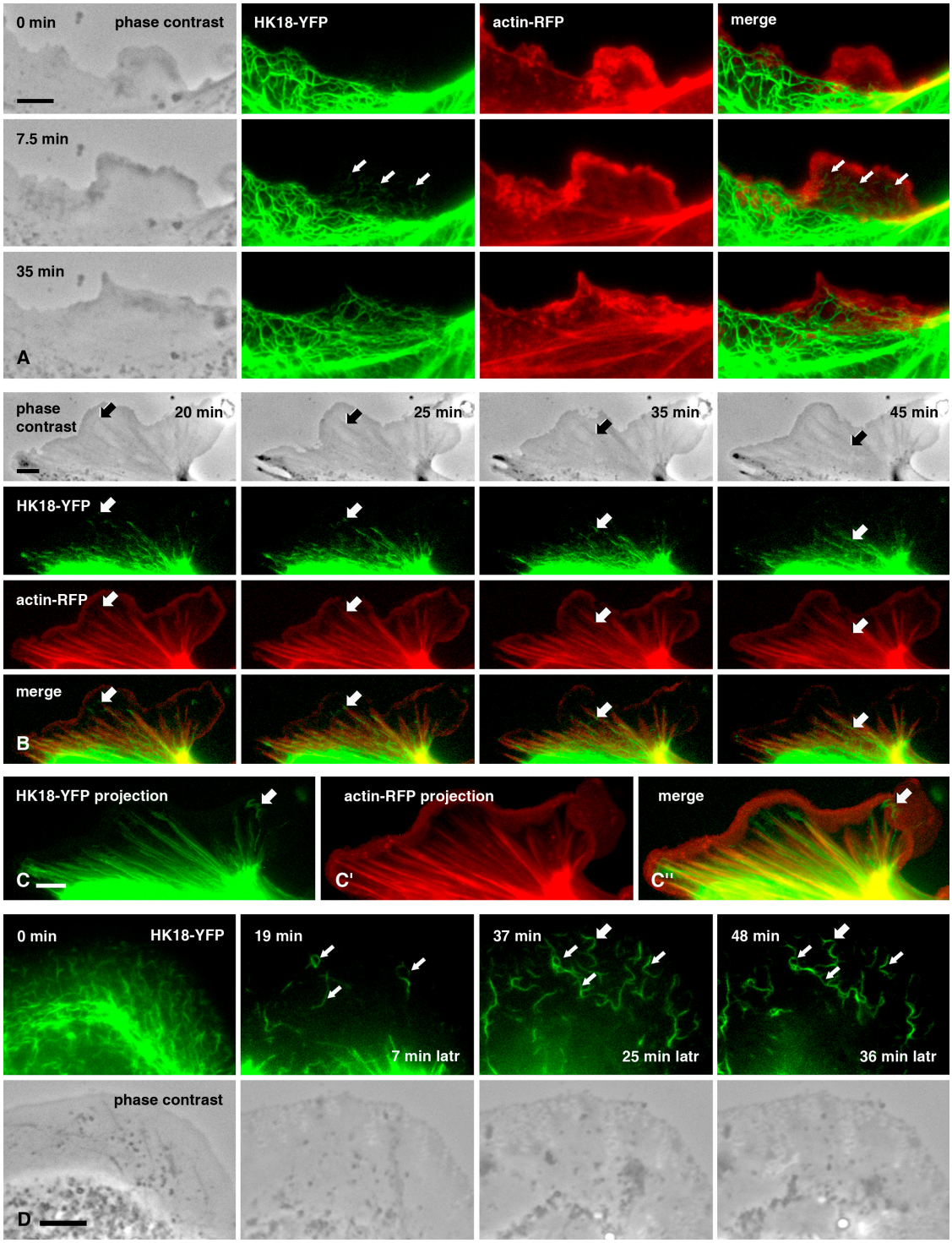

Figure 1. **Actin-dependent dynamics of KFPs in the lamellipodia of mammary epithelium–derived EpH4 cells producing HK18-YFP.** (A) Phase-contrast and fluorescence images of a time-lapse recording (Video 1) showing HK18-YFP (green) and actin-RFP (red; merge at right) in an emerging lamellipodium. Note the appearance of KFPs at 7.5 min (arrows) and their subsequent assembly into a novel IF network (35 min). (B) Micrographs taken from a time-lapse recording (Video 2) of HK18-YFP and actin-RFP epifluorescence, together with corresponding phase contrasts depicting inward-directed KFP transport along lamellipodial actin fibers (arrows). Video 2 corresponds with these images, and further demonstrates that most particles exhibit the same continuous and comparatively slow movement. (C) Projections of all 200 frames taken from either the HK18-YFP or actin-RFP channel of Video 1, along with an overlay of both (merge). The resulting overlapping lines show that KFPs move along actin fibers. One of the rarely occurring particles transported in a rapid and discontinuous fashion, probably along microtubules, is marked by an arrow. (D) HK18-YFP fluorescence and corresponding phase contrasts of a peripheral region of a cell treated with 10 μM latrunculin B (latr). Note the continued formation of KFPs and the complete inhibition of inward-directed KFP mobility (arrows; Video 3). Videos 1–3 are available at http://www.jcb.org/cgi/content/full/jcb.200511124/DC1. Bars, 5 μm.

actin-anchoring focal adhesions (FAs). Immortalized mammary epithelium–derived EpH4 cells were used, given their tendency to form large lamellipodia (Oliferenko et al., 2000). Cells were doubly transfected with cDNAs coding for human keratin 18 (HK18)–YFP and actin–red fluorescent protein (RFP) to simultaneously monitor the keratin and actin system. Fluorescence micrographs were recorded together with phase-contrast pictures of spontaneously forming lamellipodia (Fig. 1 A and Video 1, available at http://www.jcb.org/cgi/content/full/jcb.200511124/DC1). Typically, emerging lamellipodia contained abundant actin, but, at least initially, no particulate keratin fluorescence. The first KFPs appeared only a few minutes after expansion (Fig. 1 A, 7.5 min, arrows). Subsequently, more KFPs formed, which were transported inward before fusion with each other and establishment of a new network extension in the protrusion (Fig. 1 A, 35 min). We conclude that lamellipodia are regions that induce the formation of novel KF networks and, hence, contain the regulatory mechanisms and signals favoring this process.

KFPs are transported along actin stress fibers

To characterize the nature of the continuous inward transport of KFPs, we examined their mobility in relation to actin stress fibers, which are often very prominent in lamellipodia. Double-fluorescence recording of HK18-YFP and actin-RFP revealed a remarkable codistribution (Fig. 1 B). Most KFPs were seen to migrate along actin fibers (Fig. 1 B, arrows) in a continuous, inward-directed, and comparatively slow (~500 nm/min) fashion

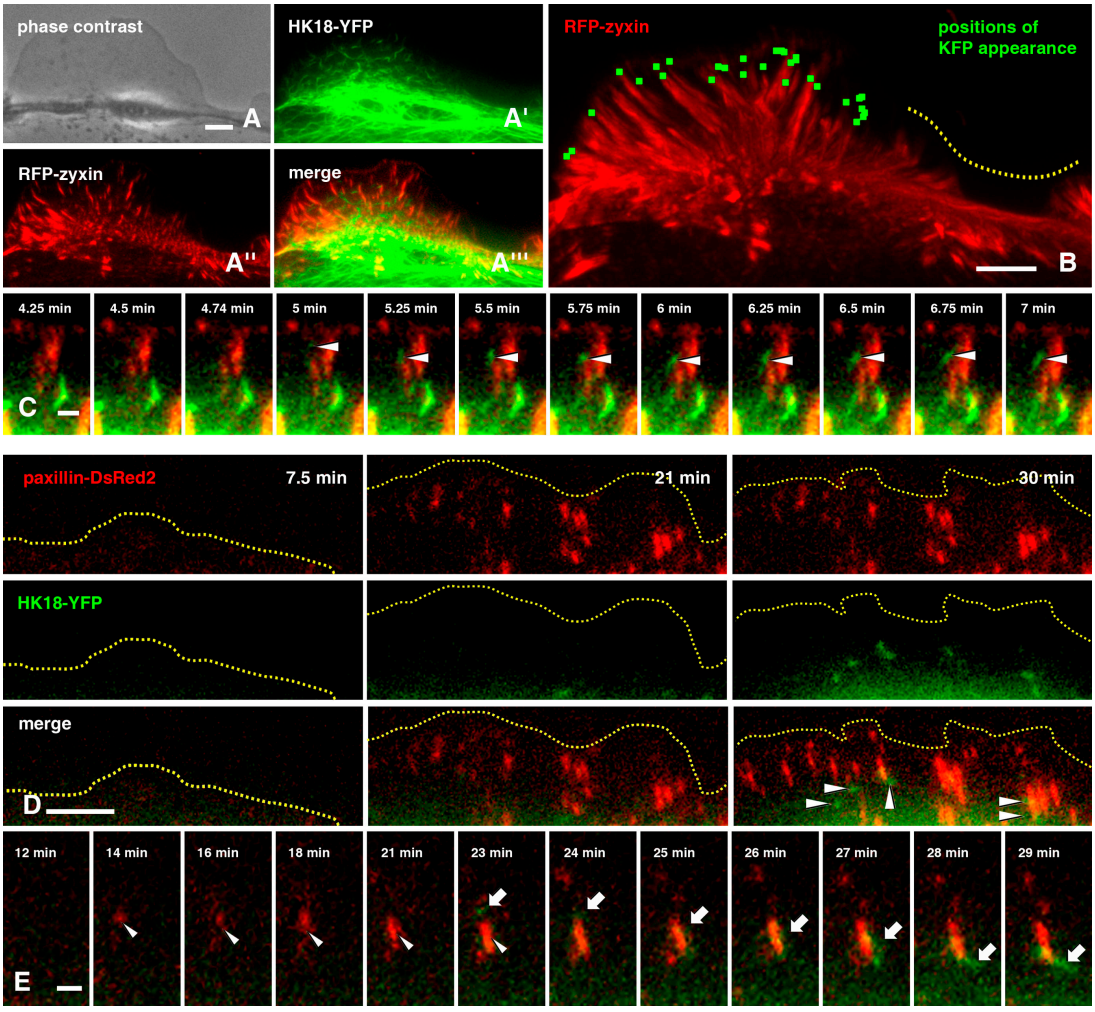

Figure 2. **Formation of KFPs in the vicinity of FAs.** (A) Phase-contrast and fluorescence images taken from a single time point of a time-lapse series (Video 4) depicting a lamellipodium of an EpH4 cell producing HK18-YFP (A') and RFP-zyxin (A''). (B) Projection of the 200 frames of the RFP-zyxin fluorescence of Video 4, together with the positions of sites where KFPs were detectable for the first time (green dots). Note that most KFP initiation sites are close to the tips of labeled FAs and that KFP formation is absent in areas without FAs (dotted line). (C) High magnification images retrieved from Video 4 highlight the formation of a KFP in the vicinity of a zyxin-positive adhesion site (cell margin at top). The KFP is first visible at 5 min (arrowhead), growing subsequently while moving toward the cell interior. (D) Fluorescence recordings taken from a time-lapse series of an EpH4 cell synthesizing HK18-YFP and paxillin-DsRed2 (Video 5). The position of the emanating plasma membrane (dotted line) was determined from phase-contrast images. Note that shortly after lamellipodial extension (7.5 min) there is no fluorescence above background, and that at 21 min paxillin-labeled FA sites have formed, but no KFPs are detectable. They appear only later, are detectable (arrows; 30 min). (E) High magnification sequence taken from Video 5 depicting the temporally staggered gradual growth of a FA (arrowhead) and subsequent appearance of an inward-moving KFP (arrow). Videos 4 and 5 are available at http://www.jcb.org/cgi/content/full/jcb.200511124/DC1. Bars: (A, B, and D) 5 μm; (C and E) 1 μm.

(Video 2, available at http://www.jcb.org/cgi/content/full/jcb.200511124/DC1), which is characteristic for actin-dependent transport (Werner et al., 2004; Wöll et al., 2005). Overlays of all frames of the keratin and actin fluorescence recordings (Fig. 1 C) resulted in both parallel and partially overlapping tracks, as would be expected for linked transport phenomena. In rare instances, however, individual KFPs that were away from stress fibers exhibited a discontinuous, bidirectional, and rapid motility (Fig. 1 C, arrow), which are the signets of microtubule-dependent transport (Wöll et al., 2005). Cells were treated with the actin polymerization inhibitor latrunculin B to further assess the importance of actin filaments for KFP dynamics. KFP transport ceased immediately, whereas KFP formation, elongation, and fusion continued (Fig. 1 D and Video 3). We conclude that the great majority of lamellipodial KFPs are transported along actin fibers. Comparable transport modes are probably also relevant to other IFs because cortical actin–dependent transport of newly synthesized neurofilament subunits occurs in axonal shafts (Rao et al., 2002; Jung et al., 2004) and growth cones (Chan et al., 2003).

KFP assembly is spatially and temporally linked to FA sites

Recruitment of newly formed KFPs usually occurred at the most peripheral tips of actin stress fibers (Fig. 1 B and Video 2), which is where they are anchored to the plasma membrane via FAs that also attach cells to the extracellular matrix (Petit and Thiery, 2000; Geiger et al., 2001; Carragher and Frame, 2004). In addition, FAs act as important signaling platforms that also affect the microtubule system (Small and Kaverina, 2003). To explore whether FAs are also determinants of KFP formation, EpH4 cells were doubly labeled with HK18-YFP and FA components such as RFP-zyxin and paxillin-DsRed2. Overall, abundant KFP formation was noted in lamellipodia containing abundant FAs, but was low in the areas between lamellipodia (Fig. 2, A and B, and Video 4, available at http://www.jcb.org/cgi/content/full/jcb.200511124/DC1). KFPs appeared remarkably close to FAs. Thus, 87% ($n = 31$) of the KFPs that formed during the 50-min recording of Video 4 were first detected within six pixels (corresponding to 0.66 μm) of a zyxin-labeled FA

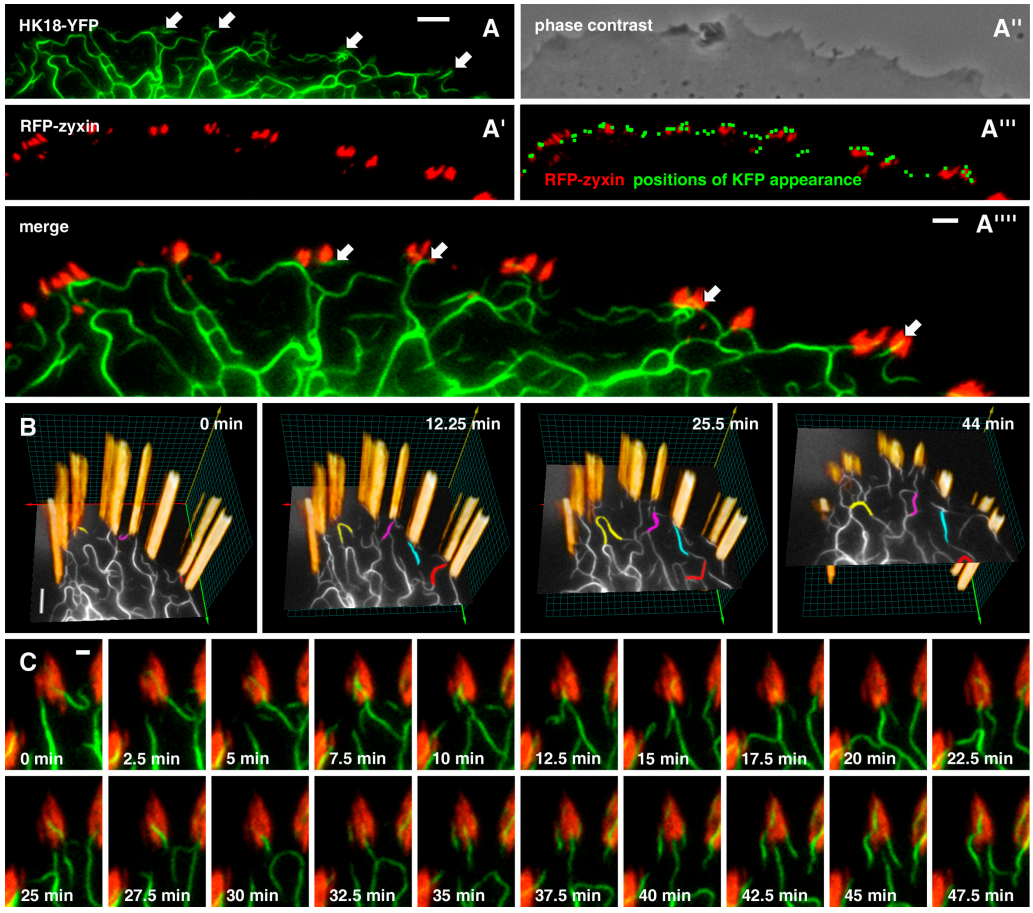

Figure 3. **Formation of KFPs in the vicinity of FAs in nonepithelial cells.** (A) Pictures of a time-lapse recording (Video 6) of the fluorescence (A, A', and A'''') and phase contrast (A'') of a SK8/18-2 cell producing fluorescent HK18-YFP (A), HK8-CFP (not depicted), and RFP-zyxin (A'). Several KFPs are visible (arrows). (A'''') Merged images of A and A' at high magnification. (A''') Projection of all 200 images recorded in the RFP-zyxin channel, together with the positions (green dots) where KFPs were first detected during the 50-min observation period. (B) Four-dimensional representation of the subdata of a time-lapse recording of another region of the cell shown in A. The red and green axes represent the image plane, whereas the yellow axis corresponds to time. RFP-zyxin fluorescence is shown in voxel representation resulting in orange rods that change only little over time as a consequence of the static nature of the FAs. Four time points of the complete sequence (Video 7) are shown and four KFPs are color-coded to highlight their dynamic behavior in relation to FAs. (C) Sequence of high magnification images demonstrating the appearance, growth, and mobility of KFPs in relation to FAs (Video 8). The cell edge is at the top. Videos 6–8 are available at http://www.jcb.org/cgi/content/full/jcb.200511124/DC1. Bars: (A and B) 5 μm; (A'''') 2 μm; (C) 1 μm.

(Fig. 2 B and Fig. S1). The high magnification images in Fig. 2 C provide an example for the tight spatial configuration of emerging KFPs and FAs. Similar images could be recorded using the early FA marker paxillin (Fig. 2, D and E and Video 5). In this instance, 35 emerging KFPs were identified, 75% (26) of which were first seen less than seven pixels away from a FA (Fig. S1). It should be kept in mind that we may not be able to detect the initially forming KFPs, but we may be able to see enlarging and, hence, increasingly fluorescent KFPs only after release from their presumptive nucleation sites. Also, cytoskeletal linker molecules are capable of bridging considerable distances of several hundred nanometers and could therefore be responsible for the detection of associated molecules outside of their anchoring platforms.

To elucidate the temporal relationship between FA formation and KFP assembly, the appearance of paxillin- and keratin-positive structures was examined in emanating lamellipodia. Dual-color time-lapse images revealed that paxillin-containing FAs were established in expanding lamellipodia before KFPs appeared in close proximity (Fig. 2, D and E and Video 5).

FA-dependent KFP assembly also occurs in nonepithelial cells

To find out whether FA-associated KFP formation is determined by cell-specific factors, analyses were extended to nonepithelial SW13 cells lacking cytoplasmic IFs. These cells form extended cytoplasmic KF networks when transfected with fluorescent protein–tagged HK8 and HK18 in stable cell clone SK8/18-2 (Windoffer et al., 2004; Wöll et al., 2005). Because the entire keratin system is solely composed of fluorescent polypeptides, SK8/18-2 cells are particularly suited for detection of very small keratin particles. In perfect agreement with the results obtained in epithelial cells, multicolor time-lapse imaging of HK18-YFP and RFP-zyxin revealed a tight correlation between KFP formation and FAs (Fig. 3 A and Video 6, available at http://www.jcb.org/cgi/content/full/jcb.200511124/DC1). Visual assignment of all KFP initiation events ($n = 83$) onto the zyxin images further demonstrated that 77% (64) were positioned within six pixels of each other (Fig. 3 A'", and Fig. S1). The stability of FAs in these cells allowed us to prepare multidimensional representations in which the surface of the labeled FAs drawn in time space were correlated with the two-dimensional fluorescence patterns at different time points (Fig. 3 B). Animation of these time series (Video 7) further highlights the emergence of forming KFPs from FAs and their subsequent integration into the peripheral KF network. This process repeats itself multiple times, with single FA sites serving as platforms for the formation of several KFPs (Fig. 3 C and Video 8).

Epidermolysis bullosa simplex–type mutations do not prevent FA-dependent KFP formation

It was recently shown that KF network formation is inhibited in cells producing mutant keratins that are known to cause the skin disorder epidermolysis bullosa simplex, although KFPs are still formed in the cell periphery (Werner et al., 2004). These KFPs, however, fail to elongate, and, instead, enlarge into short-lived spheroid granules that move continuously in an actin-dependent process toward the cell center and disintegrate into soluble material at a distinct transition zone. When we transfected paxillin-DsRed2 cDNAs into epithelial cell lines, producing the fluorescent HK14 mutants enhanced YFP(EYFP)-$K14_{R125C}$, we observed that paxillin-labeled FAs were prominent initiation sites from which KFPs emerged (Fig. 4 A and Video 9, available at http://www.jcb.org/cgi/content/full/jcb.200511124/DC1). Overlay of visually assigned sites of KFP formation onto paxillin-DsRed2 images further supported their tight spatial relationship (Fig. 4 B) with 93% (246) of initiation events ($n = 264$) detected within 6 pixels of FAs (Fig. S1). Repeated granule formation from the same FAs was noted every 1.5–4 min (Fig. 4 C; Video 9).

Talin short hairpin RNA (shRNA) interferes with KFP formation

Cells were treated with shRNAs directed against FA components to directly evaluate the contribution of FAs to KFP formation. Talin-specific shRNAs induced retraction of the KF network around the nucleus and depletion of KFPs in peripheral regions, whereas cells transfected with control shRNAs did not show these alterations (Fig. 5, A and B). Similarly, cells synthesizing mutant keratins retained only the residual perinuclear filament system and lacked the characteristic peripheral keratin granules (Fig. 5, C and D). The specificity and efficiency of talin down-regulation was confirmed by talin immunofluorescence in each instance (Fig. S2, available at http://www.jcb.org/cgi/content/full/jcb.200511124/DC1).

Conclusions

We have recently suggested that certain submembraneous sites are important for KF formation and turnover, thereby directing the assembly machinery into cell regions requiring major IF restructuring (Windoffer and Leube, 2001; Windoffer et al., 2004). The current study identifies FAs as perfectly suited candidates to perform such tasks. FAs are abundant and prominent entities at the extracellular matrix–cell interface, providing complex platforms that mediate structural and signaling functions. The evidence presented in this study for a tight linkage of these sites to KF formation, in combination with well established knowledge about the crucial functions of FAs for the actin system (Petit and Thiery, 2000; Geiger et al., 2001; Carragher and Frame, 2004) and recent studies linking FAs to the microtubule network in an intricate reciprocal cross talk (Kaverina et al., 1998; Krylyshkina et al., 2003), assign even more important functions to these sites than hitherto anticipated and place them as central regulators ensuring coordination of the entire cytoskeleton in situations of polarized cell shape changes. A finely adjustable program appears to start in lamellipodia once FAs have formed, beginning with stress fiber recruitment, followed by several poorly characterized transition states, each of which could be subject to feedback control with the intra- and extracellular environment, eventually ending up in the formation of a stabilizing IF cytoskeleton (Ridley et al., 2003). In this way, polarized reorganization of the cytoskeleton is accomplished, resulting in directed movement and relocation of

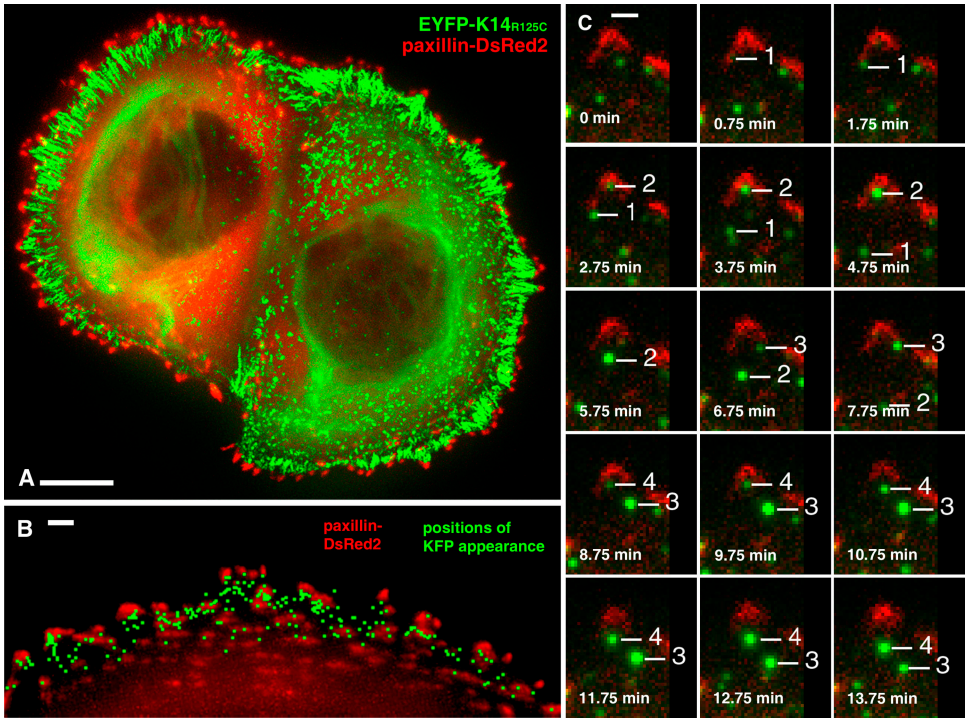

Figure 4. **Formation of mutant keratin particles at FAs.** Time-lapse recording of MCF7 cells expressing mutant keratin EYFP-K14$_{R125C}$ and paxillin-DsRed2 (Video 9). (A) Projection of 100 frames of both fluorescence channels recorded in 15-s intervals. Note that the peripheral FAs remain quite stable, whereas emerging keratin granules move continuously from FAs to the cell interior, to a distinct transition zone where they disassemble. (B) Projection of all paxillin-DsRed2 images together with the positions (green dots) where KFPs appeared first. (C) High magnification images from Video 9 showing the consecutive appearance of four keratin granules from a single FA. Video 9 is available at http://www.jcb.org/cgi/content/full/jcb.200511124/DC1. Bars: (A) 10 μm; (B) 2 μm; (C) 1 μm.

the trailing part of the cell, which would have to undergo similarly coordinated disassembly processes. Such a hierarchical organization of the cytoskeletal systems is also supported by observations during epithelial sheet formation, when zippering of actin-anchoring punctate adhesions in fingerlike protrusions of epidermal keratinocytes precede keratin/desmosome-mediated clamping adhesion (Vasioukhin et al., 2000).

The uncovered tight relationship between KFPs and FAs reflects basic cellular properties, as it is detectable in cells of different origin and is also maintained in cells producing mutant keratins. The same phenomena were also noted using other keratins and cell lines (Video 10, available at http://www.jcb.org/cgi/content/full/jcb.200511124/DC1). Furthermore, we would like to suggest that the observed mechanisms are not restricted to keratin IFs, but also apply to other IF types. Evidence for this notion was provided in endothelial cells producing fluorescent vimentin and β3 integrin–labeled FAs (Tsuruta and Jones, 2003). The observed dynamic colocalization supports the possibility that FAs are sites of vimentin filament nucleation and/or assembly. In summary, FAs may be the long sought after IF-organizing centers.

Materials and methods

DNA cloning

Cloning of a cDNA coding for fusion protein HK18-YFP was previously described (Strnad et al., 2002). To prepare hybrid cDNAs coding for HK14 fused to EYFP, K14 was amplified from a K14 cDNA (provided by V. Nimrich, German Cancer Research Center, Heidelberg, Germany) using the amplimers 00–52 5′-AAA AAG CTT ATG ACT ACC TGC AGC CGC CAG-3′ and 00–53 5′-AAA GGA TCC GGG TTC TTG GTG CGA AGG ACC TG-3′; the resulting fragment was cloned into the HindIII–BamHI sites of pEYFP-N1 (CLONTECH Laboratories, Inc.), thereby generating plasmid HK14-YFP. Plasmid HK14$_{R125C}$-YFP was created by substituting the HindIII–Asp718 fragment with the corresponding fragment of EYFP-K14$_{R125C}$ (Werner et al., 2004). A RFP-zyxin–encoding construct was provided by A. Huttenlocher (University of Wisconsin, Madison, WI; Bhatt et al., 2002). For preparation of actin-RFP, the cDNA for monomeric RFP (Campbell et al., 2002) was PCR amplified using primers 03–88 5′-AGA TCC GCT AGC CGA TAA GGA TCC GAT GGC C-3′ and 03–89 5′-AGC TCG AGA TCT GGC GCC GGT GGA GTG GC-3′. The NheI–BglII–cleaved PCR product was used to substitute the EGFP-encoding fragment in plasmid pEGFP-actin (CLONTECH Laboratories, Inc.). Construct paxillin-pDsRed2-N1 coding for paxillin-DsRed2 was provided by A. Horwitz (University of Virginia School of Medicine, Charlottesville, VA; Webb et al., 2004).

shRNA constructs

For the shRNA cloning plasmid, pTER (van de Wetering et al., 2003) was first modified by introducing a 1,379-bp SpeI–XbaI–limited, CMV promotor–driven, EGFP-encoding fragment that was PCR amplified from pEGFP-C3 (CLONTECH Laboratories, Inc.; prepared and provided by L. Griffin and E. Bockamp, Institute of Toxicology, Johannes Gutenberg University, Mainz, Germany). The EGFP-encoding fragment of the resulting plasmid, pTER-EGFP, was then exchanged for a 765-bp NheI–XbaI–cleaved mRFP fragment that was amplified from the actin-RFP–encoding plasmid (see previous section) with primers 03–88 and 04–72 5′-AAA GCG GCC GCT TAG GCG CCG GTG GAG TGG C-3′, thereby generating the plasmid pTER-mRFP. Synthetic oligonucleotides were subsequently inserted downstream of the H1 promotor into the BglII–HindIII sites. For talin-specific constructs, the oligonucleotides talin_1_sense 5′-GAT CCC GGC ACT CAC TGG AAC CAT TTT CAA GAG AAA TGG TTC CAG TGA GTG CCT TTT TGG AAA-3′ and control_1_antisense 5′-AGC TTT TCC AAA AAG GCA CTC ACT GGA ACC ATT TCT CTT GAA AAT GGT TCC AGT GAG TGC

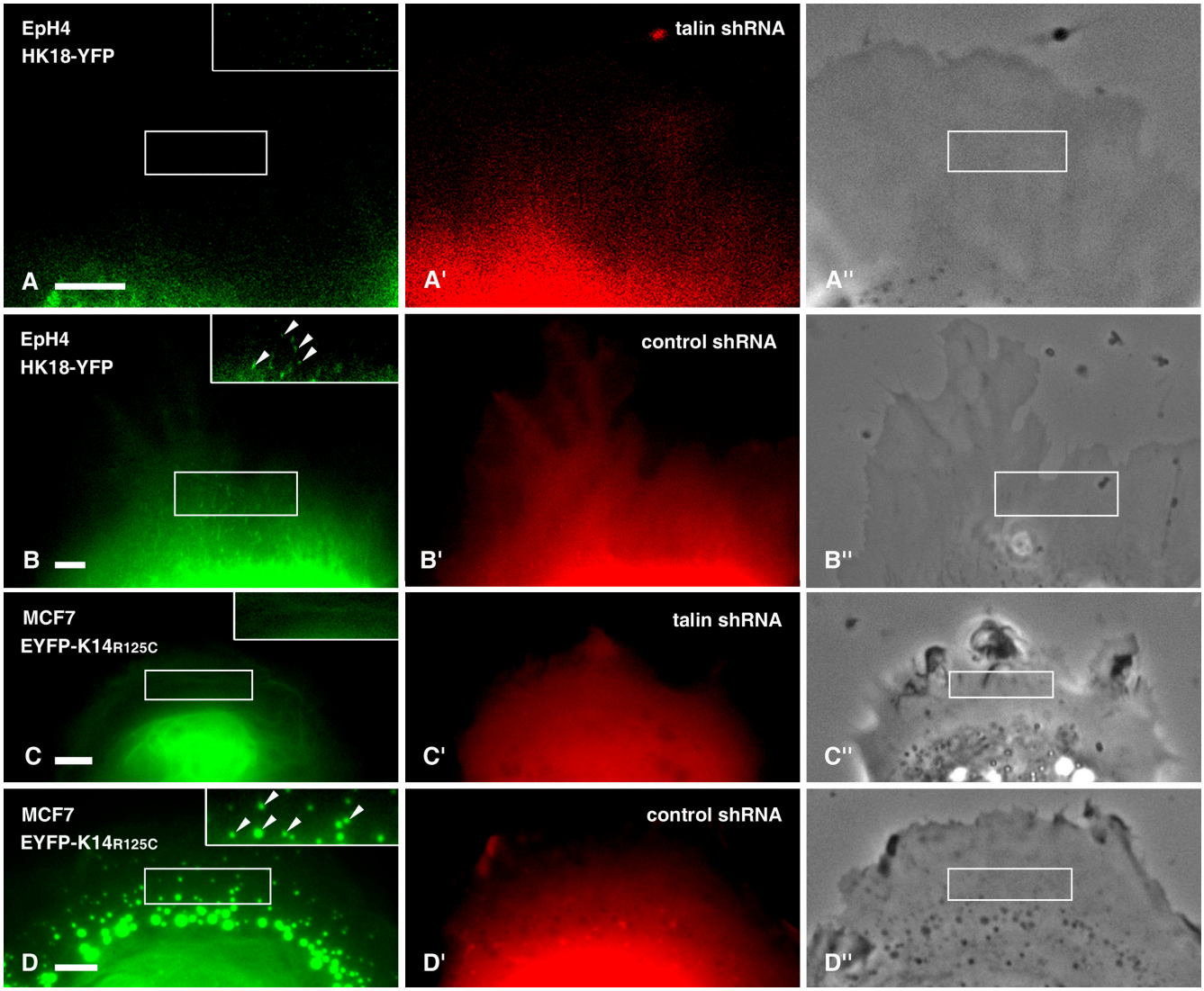

Figure 5. **Inhibition of KFP formation in the presence of talin shRNA.** (A–D) Fluorescence micrographs and corresponding phase contrasts of EpH4 cells synthesizing HK18-YFP (A and B) and MCF7 cells producing EYFP-K14$_{R125C}$ (C and D), together with either talin-specific shRNA (A and C) or control shRNA (B and D). shRNA-producing cells are identified by linked RFP- (A' and C') or CFP-expression (pseudocolor in B' and D'). A'' and D'' are the corresponding phase contrasts. Note the reduction of wild-type and mutant KFPs in the peripheral cytoplasm of talin shRNA-treated cells. Arrowheads, KFPs. Bars, 5 μm (insets, 150% enlargement of boxed areas).

CGG-3′, and the control oligonucleotides, control_1_sense 5′-GAT CCC GGC ACT CAC TGG AAC CAT TTT CAA GAG AAA TGT TCC AGT GAG TGC CGG GAT CTA-3′ and control_1_antisense 5′-AGC TTA GAT CCC GGC ACT CAC TGG AAC ATT TCT CTT GAA AAT GGT TCC AGT GAG TGC CGG-3′, which differed only slightly from the talin oligonucleotides, were used. Complementary oligonucleotides (100 μM of each) were annealed by incubation for 5 min at 95°C, followed by incubation at 75°C for 15 min in annealing buffer (100 mM potassium acetate, 30 mM Hepes-KOH, pH 7.4, and 2 mM magnesium acetate). In some instances, the EGFP-encoding fragment of pTER-EGFP was removed with AgeI–PmeI and substituted with the corresponding ECFP-encoding fragment of plasmid pECFP-N1 (CLONTECH Laboratories, Inc.), resulting in plasmid pTER-ECFP. Subsequently, cloned shRNA-encoding oligonucleotides were excised with HindIII–EcoRI from the pTER-mRFP–derived plasmids and inserted into pTER-ECFP. The efficiency of shRNA-mediated inhibition of talin production was evaluated with specific talin antibodies (clone 8D4; Sigma-Aldrich) 48 h after plasmid transfection in formaldehyde-fixed cells.

Cell culture

SK8/18-2 (Wöll et al., 2005) and MT5K14-26 (provided by N. Werner and T. Magin, Universitätsklinikum, Bonn, Germany; Werner et al., 2004) were cultured as previously described. The spontaneously immortalized mouse mammary epithelial cell line EpH4 was provided by L. Huber (Universität Innsbruck, Innsbruck, Austria) and H. Beug (Institute of Molecular Pathology, Wein, Austria; Oliferenko et al., 2000). It was maintained in DME with high glucose and 10% fetal bovine serum in a humidified incubator at 37°C with 5% CO_2. Cells were transfected with the help of Lipofectamine 2000 reagent (Invitrogen).

Live-cell imaging

For time-lapse live-cell fluorescence recording, cells were grown in glass-bottom Petri dishes (MatTek Corp.), and phenol-free Hank's medium (Invitrogen) was used during imaging. Pictures were recorded by epifluorescence microscopy using an inverse microscope (model IX 70; Olympus) and an attached slow scan camera (model IMAGO; TILL Photonics) as previously described (Windoffer et al., 2002). The microscope was kept in a closed chamber at 37°C. A 60×, 1.4 NA, oil immersion objective was used, and fluorescence excitation with a monochromatic light of 500 or 570 nm was accomplished with a monochromator (TILL Photonics). At each time point of the time-lapse sequences YFP, RFP, and phase-contrast images were acquired successively within 1.5 s (TILLvisION software; TILL-Photonics). The resulting image sequences were edited with ImagePro Plus

(Media Cybernetics). Raw data were cropped and lookup table–adjusted, and the fluorescence channels were color-coded and combined for optimal presentation. To remove residual bleed-through of the RFP signal into the YFP channel, unmixing was performed in some instances (Fig. 1 A and Video 1) by subtracting the corrected (F = 0.12) red channel (R) from the green channel (G) according to UMIX = G – (R × F). Amira software (Mercury Computer Systems) was used to generate the 3D visualization of fluorescence in Fig. 3 B.

Localization of KFP appearance

The cropped and lookup table–adjusted fluorescence image stacks were edited using Amira software. The x, y, and t positions of the first appearance of KFPs were located by visual inspection at high magnification and manually tagged into the frames. A positive score was only assigned when fluorescence was significantly above the diffuse background (probably corresponding to the soluble keratin pool) in at least four adjacent pixels (one pixel covers ~120 × 120 nm), and when particle growth could be unambiguously detected in subsequent frames. The manually tagged positions of KFP appearance were transferred into the RFP images depicting the location of labeled FA sites. The distances between the yellow fluorescent KFPs to the next red fluorescent FAs were measured and analyzed in a spreadsheet. The tags were projected into one frame and overlaid onto the projected RFP recordings.

Online supplemental material

Most videos are represented, at least in part, in the figures. Video 1 (Fig. 1 A) depicts the establishment of a novel KF network in a newly formed lamellipodium. Video 2 (Fig. 1 B) demonstrates the transport of KFPs along actin stress fibers in a lamellipodium. Video 3 (Fig. 1 D) records the peripheral keratin fluorescence in a cell treated with latrunculin B. Videos 4 and 5 (Fig. 2) show the appearance of KFPs in close neighborhood to FAs that are either labeled with RFP-zyxin (Video 4) or paxillin-DsRed2 (Video 5). Videos 6–8 (Fig. 3) document the emergence of KFPs from RFP-zyxin–labeled FAs in nonepithelial SK8/18-2 cells at low magnification as a tableau (Video 6), in an animated time-space reconstruction (Video 7), and at high magnification (Video 8). Video 9 (Fig. 4) presents an image series of MCF7 cells producing fluorescent keratin 14 mutants together with paxillin-DsRed2. Video 10 is a composite of two recordings (no corresponding figures) of either HK14-YFP and paxillin-DsRed2 (top) or $HK14_{R125C}$-YFP and RFP-zyxin (bottom) in EpH4 cells. In addition, Fig. S1 provides quantitative data on the spatial relationship between KFP formation and FAs (Figs. 2–4 and Videos 4–6 and 9). Fig. S2 presents control data to the experiments depicted in Fig. 5. Online supplemental materials are available at http://www.jcb.org/cgi/content/full/jcb.200511124/DC1.

We thank Drs. Anna Huttenlocher, Alan Horwitz, Louise Griffin, Ernesto Bockamp, Lukas Huber, Hartmut Beug, Nicola Werner, and Thomas Magin for providing cDNAs and cell lines. We are also grateful to Drs. Yuko Miyamato and Rudy Juliano for sharing unpublished information on talin siRNAs, and to Ursula Wilhelm for expert technical help.

This work was supported by the German Research Council (LE 566/7).

Submitted: 28 November 2005
Accepted: 4 April 2006

References

Bhatt, A., I. Kaverina, C. Otey, and A. Huttenlocher. 2002. Regulation of focal complex composition and disassembly by the calcium-dependent protease calpain. *J. Cell Sci.* 115:3415–3425.

Campbell, R.E., O. Tour, A.E. Palmer, P.A. Steinbach, G.S. Baird, D.A. Zacharias, and R.Y. Tsien. 2002. A monomeric red fluorescent protein. *Proc. Natl. Acad. Sci. USA*. 99:7877–7882.

Carragher, N.O., and M.C. Frame. 2004. Focal adhesion and actin dynamics: a place where kinases and proteases meet to promote invasion. *Trends Cell Biol.* 14:241–249.

Chan, W.K., J.T. Yabe, A.F. Pimenta, D. Ortiz, and T.B. Shea. 2003. Growth cones contain a dynamic population of neurofilament subunits. *Cell Motil. Cytoskeleton*. 54:195–207.

Coulombe, P.A., and M.B. Omary. 2002. 'Hard' and 'soft' principles defining the structure, function and regulation of keratin intermediate filaments. *Curr. Opin. Cell Biol.* 14:110–122.

Geiger, B., A. Bershadsky, R. Pankov, and K.M. Yamada. 2001. Transmembrane crosstalk between the extracellular matrix–cytoskeleton crosstalk. *Nat. Rev. Mol. Cell Biol.* 2:793–805.

Helfand, B.T., L. Chang, and R.D. Goldman. 2003. The dynamic and motile properties of intermediate filaments. *Annu. Rev. Cell Dev. Biol.* 19:445–467.

Herrmann, H., and U. Aebi. 2004. Intermediate filaments: molecular structure, assembly mechanism, and integration into functionally distinct intracellular Scaffolds. *Annu. Rev. Biochem.* 73:749–789.

Herrmann, H., M. Hesse, M. Reichenzeller, U. Aebi, and T.M. Magin. 2003. Functional complexity of intermediate filament cytoskeletons: from structure to assembly to gene ablation. *Int. Rev. Cytol.* 223:83–175.

Jung, C., T.M. Chylinski, A. Pimenta, D. Ortiz, and T.B. Shea. 2004. Neurofilament transport is dependent on actin and myosin. *J. Neurosci.* 24:9486–9496.

Kaverina, I., K. Rottner, and J.V. Small. 1998. Targeting, capture, and stabilization of microtubules at early focal adhesions. *J. Cell Biol.* 142:181–190.

Krylyshkina, O., K.I. Anderson, I. Kaverina, I. Upmann, D.J. Manstein, J.V. Small, and D.K. Toomre. 2003. Nanometer targeting of microtubules to focal adhesions. *J. Cell Biol.* 161:853–859.

Leung, C.L., K.J. Green, and R.K. Liem. 2002. Plakins: a family of versatile cytolinker proteins. *Trends Cell Biol.* 12:37–45.

Oliferenko, S., I. Kaverina, J.V. Small, and L.A. Huber. 2000. Hyaluronic acid (HA) binding to CD44 activates Rac1 and induces lamellipodia outgrowth. *J. Cell Biol.* 148:1159–1164.

Petit, V., and J.P. Thiery. 2000. Focal adhesions: structure and dynamics. *Biol. Cell.* 92:477–494.

Rao, M.V., L.J. Engle, P.S. Mohan, A. Yuan, D. Qiu, A. Cataldo, L. Hassinger, S. Jacobsen, V.M. Lee, A. Andreadis, et al. 2002. Myosin Va binding to neurofilaments is essential for correct myosin Va distribution and transport and neurofilament density. *J. Cell Biol.* 159:279–290.

Ridley, A.J., M.A. Schwartz, K. Burridge, R.A. Firtel, M.H. Ginsberg, G. Borisy, J.T. Parsons, and A.R. Horwitz. 2003. Cell migration: integrating signals from front to back. *Science*. 302:1704–1709.

Small, J.V., and I. Kaverina. 2003. Microtubules meet substrate adhesions to arrange cell polarity. *Curr. Opin. Cell Biol.* 15:40–47.

Strnad, P., R. Windoffer, and R.E. Leube. 2002. Induction of rapid and reversible cytokeratin filament network remodeling by inhibition of tyrosine phosphatases. *J. Cell Sci.* 115:4133–4148.

Tsuruta, D., and J.C. Jones. 2003. The vimentin cytoskeleton regulates focal contact size and adhesion of endothelial cells subjected to shear stress. *J. Cell Sci.* 116:4977–4984.

van de Wetering, M., I. Oving, V. Muncan, M.T. Pon Fong, H. Brantjes, D. van Leenen, F.C. Holstege, T.R. Brummelkamp, R. Agami, and H. Clevers. 2003. Specific inhibition of gene expression using a stably integrated, inducible small-interfering-RNA vector. *EMBO Rep.* 4:609–615.

Vasioukhin, V., C. Bauer, M. Yin, and E. Fuchs. 2000. Directed actin polymerization is the driving force for epithelial cell-cell adhesion. *Cell*. 100:209–219.

Webb, D.J., K. Donais, L.A. Whitmore, S.M. Thomas, C.E. Turner, J.T. Parsons, and A.F. Horwitz. 2004. FAK-Src signalling through paxillin, ERK and MLCK regulates adhesion disassembly. *Nat. Cell Biol.* 6:154–161.

Werner, N.S., R. Windoffer, P. Strnad, C. Grund, R.E. Leube, and T.M. Magin. 2004. Epidermolysis bullosa simplex-type mutations alter the dynamics of the keratin cytoskeleton and reveal a contribution of actin to the transport of keratin subunits. *Mol. Biol. Cell.* 15:990–1002.

Windoffer, R., and R.E. Leube. 2001. De novo formation of cytokeratin filament networks originates from the cell cortex in A-431 cells. *Cell Motil. Cytoskeleton*. 50:33–44.

Windoffer, R., M. Borchert-Stuhltrager, and R.E. Leube. 2002. Desmosomes: interconnected calcium-dependent structures of remarkable stability with significant integral membrane protein turnover. *J. Cell Sci.* 115:1717–1732.

Windoffer, R., S. Wöll, P. Strnad, and R.E. Leube. 2004. Identification of novel principles of keratin filament network turnover in living cells. *Mol. Biol. Cell*. 15:2436–2448.

Wöll, S., R. Windoffer, and R.E. Leube. 2005. Dissection of keratin dynamics: different contributions of the actin and microtubule systems. *Eur. J. Cell Biol.* 84:311–328.